Using Mie scattering theory to debubble seismic airguns

Joseph Jennings and Shuki Ronen

ABSTRACT

Airgun signatures contain a main pulse and then a few bubble oscliations. A process called designature or debubble such signatures into a broad band pulse. We prefer to do as much as possible with deterministic designature and leave as little as possible to statistical deconvolution. Air gun manufacturers provide a library of signatures under various conditions. However, the conditions are not well known. Near field hyderophones record the airguns. However, the near field hydrophones record all airguns in the array, and their data are contaminated by waves that do not radiate to the far field. Current methods that estimate the contribution of each airgun to the far field require inverting for a large number of parameters. In this report, we propose another a deterministic deconvolution method based on theory from Mie scattering. Our method is less sensitive to near field noise and requires only seven parameters. Instead of a linear inversion with thousands of unknowns, we have a non linear inversion with a small number of unknowns. We have encouraging results that demonstrate the potential of using Mie scattering theory for deterministic debubbling.

INTRODUCTION

The most commonly used source in marine reflection seismic surveys is an airgun. In order to transmit acoustic waves into the subsurface, airguns release a pulse of high pressure air into the water. The pulse generates an acoustic wave, similar to a champagne bottle that is uncorked. The air expands to a bubble and loses pressure. When the pressure in the bubble gets to the ambient pressure of the water, the bubble starts slowing down its expansion. Due to the inertia of the water, the bubble continues to expand and the pressure inside the bubble is lower than ambient. At some time, the bubble reaches a maximal size and starts collapsing and the pressure in the bubble starts increasing. When the pressue in the bubble reaches ambient pressure the collapse starts slowing down. Some time later the bubble reaches a minimal size and starts expanding again. Bubbles from airgun oscillate many times as they go up. Typical bubble periods are 50 to 200 milliseconds. Typical depth of airguns under the sea surface is 5-15 meters. The time it takes the bubbles to reach the surface is much longer. The bubbles radiate acoustic waves as they oscillate. As energy is radiated out of the bubble the magnitude of the oscillations diminishes.

The acoustic waves that are radiated by the bubbles go in all directions. The upgoing waves reflect from the surface and follow the waves radiated down. The surface reflection is called the source ghost. The acoustic waves, including main pulse, bubble and ghosts, propagate down through the overburden, are reflected from targets, propagate up through the overburden, are usually ghosted again near the receiver, and eventually are recorded and become data. The convolutional model of a seismic trace is described by Figure 1. To find the reflectivity that best fits the data all filters must be undone. In this paper we focus on the coupling of the Source Force to the acoustic waves which we denote as Bubble. In practice, undoing the filters denoted as Bubble and Ghosts are bundled to what is called deconvolution. To show the effects of Bubble and Source Ghost we present data from a far field hydrophone in Figure 2(a). In this example all other effects are negligible. This figure shows the wavelets and the spectra of two shots at two different depths from the same airgun with the same volume and the same pressure. The Bubble and the Source Ghost filters depend on the depth. Ghosting also depends on the angle (not shown in Figure 2(a) in which both traces have the same angle).

Figure 1: The convolutional model of seismic data. The purpose of the seismic method is to estimate the reflectivity. All other physical filters must be accounted for. In this paper we focus on deterministic methods for debubbling. [**NR**]

Deconvolution methods can be grouped as statistical and deterministic. Statistical deconvolution methods assume that the reflectivity is white. The risk is that when it is not white, statistical deconvolution will force it to be white and in the process may remove reflectors that it finds predictable from earlier reflectors. For this reason it is useful to do as little as possible with statistical deconvolution after doing as much as possible with deterministic methods.

Deterministic methods can be grouped into those that are based on library signatures and those that depend on near field hydrophones. Library methods rely on signatures that are based on data similar to those in Figure 2(a) but after deghosting. A problem with library methods is that the same airguns, with the same library signatures, vary from shot to shot because of variable depth, ambiance, and most importantly mechanical issues. In Figure 3 we present data that shows the variations of airgun signatures. There is no way the library signature can account for the variations in the actual signatures.

Near-field hydrophones (NFHs) record data shot by shot. Each NFH is near an airgun, but it also records the other airguns in the array. To estimate the notional signature of each gun, Ziolkowski et al. (1982) developed an inversion method in which unknown notional signatures are fit to NFH data. This is a linear inversion with thousands of equations and as many unknowns, assuming that each airgun has one NFH.

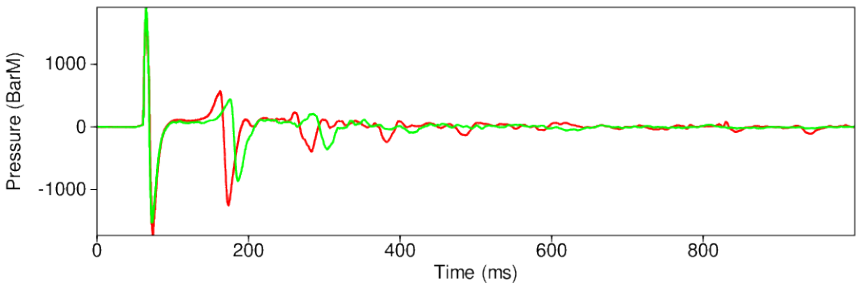

(a)

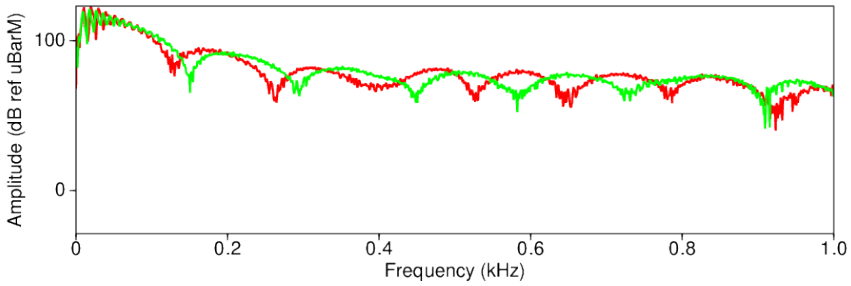

(b)

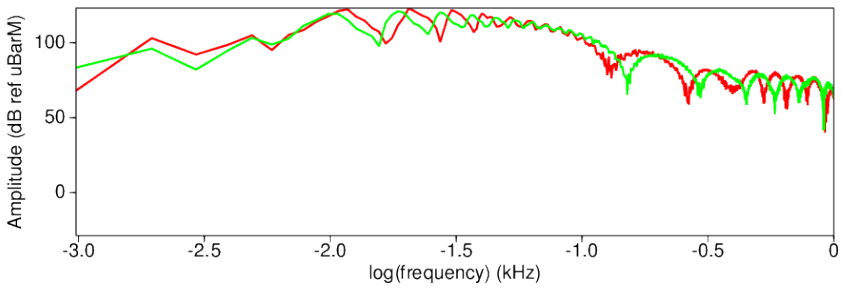

(c)

Figure 2: Far field hydrophone data (a) and their amplitude spectra in frequency (b) and log frequency (c). The data were acquired in a lake. The hydrophone was about 75 meters below the source. The bottom of the lake was about 120 meters under the hydrophone. The red trace is from an airgun at a depth of about 7 meters below the lake surface. The green trace is from the same airgun deployed at a depth of about 5 meters below the lake surface. The Bubble is dominant up to about 100Hz and the Source Ghost is dominant above 100 Hz. In the time domain (a) the deeper source has a longer delay time of the ghost and a shorter bubble period. In the frequency domain (b and c) the deeper source has a lower ghost notch frequency and a higher bubble frequency. The fundamental bubble frequency is about 9 Hz at 5 meters and about 11 Hz at 7m. The fundamental ghost notch frequency is 150 Hz at 5m and 125 Hz at 7m. Data courtesy of Dolphin Geophysical and Chelminski Associates. [**ER**]

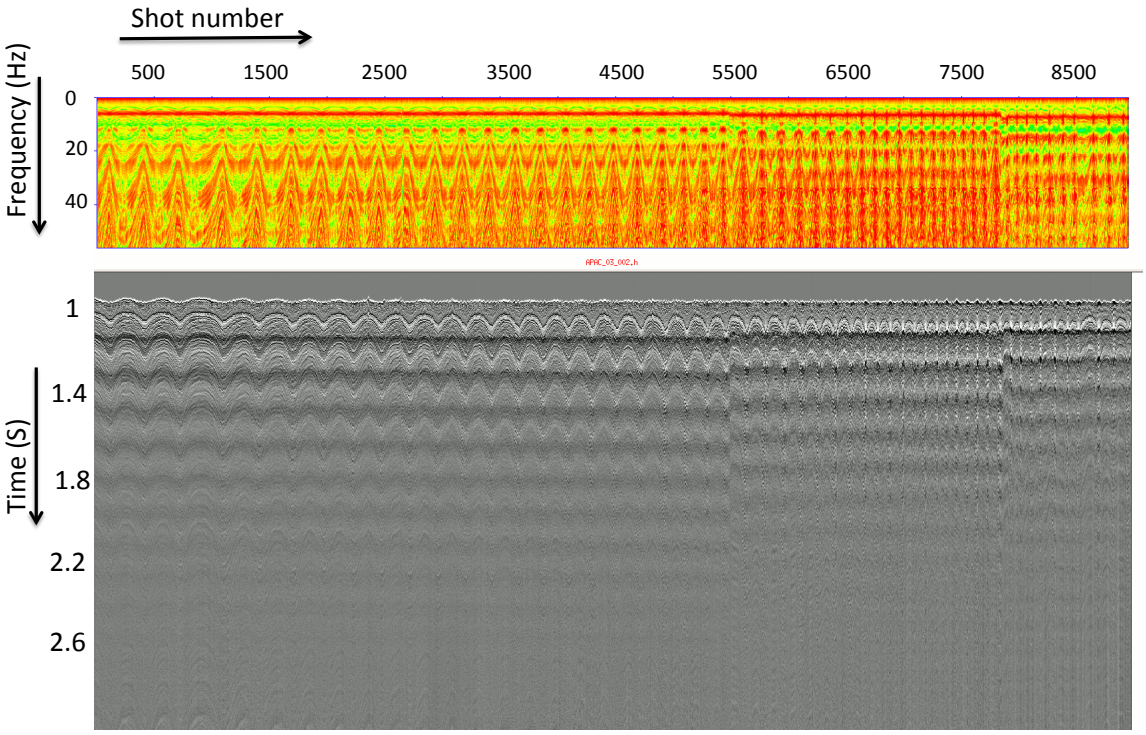

Figure 3: A common receiver gather from an ocean bottom node above the Forties oil field in the North Sea. The gather shows 9000 traces shot over a period of about 24 hours. The horizontal axis is shot number. Amplitude spectrum above and time domain below. The vertical axes are frequency and time. The data have been hyperbolically moved out, so the direct arrivals are approximately flat. The bubble period is about 100 miliseconds. The flat events are the bubble oscilations; the bubble is not affected by the angle. Other events, that are mainly multiples of reflections are affected by angle and are not flat. Note the changes in the bubble signature. One change at about shots 5500 is the start of an airleak. Hence loss of pressure. The second change at about shot 7800 is one airgun that was disconnected. Hence loss of volume. The bubble period decreased with each change. The bubble frequency increased. Data courtesy of Apache North Sea. [**NR**]

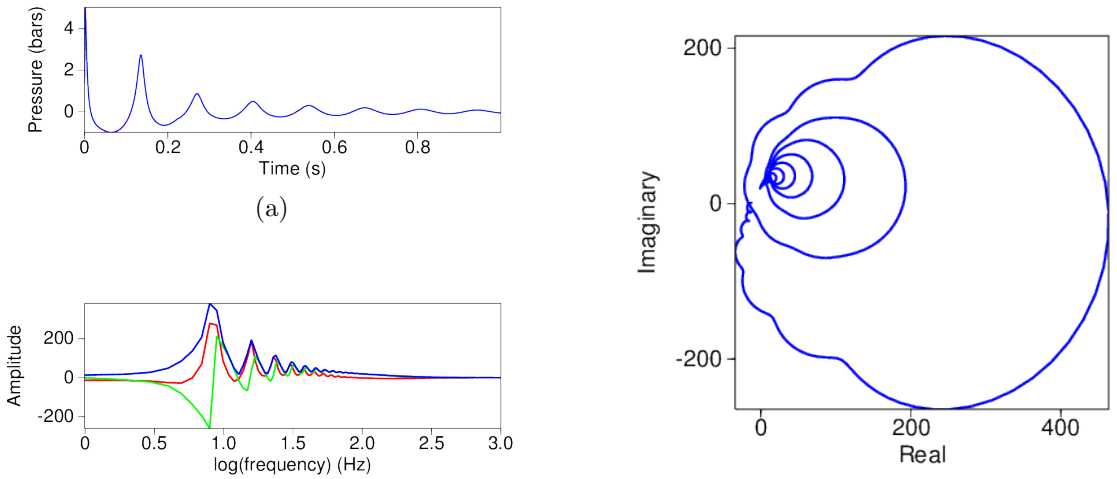

Figure 4: Analysis of the library airgun signature. (a) Time domain wavelet taken from the library. Time gate is limited to one second. (b) its real part (red), imaginary part (green), amplitude spectrum (blue). The frequency band is low-limited to 1 Hz by the time gate and high-limited to 1kH which is the Nyquist frequency of 0.5 millisecond sampling interval. (c) complex hodogram which is a cross plot of the real and imaginary parts. Note from the hodogram and the real part that the signal is primarily positive real. joseph1/. nucleus-raw,reimmag,nucleus-hodo [**ER**]

NFH measure variations from shot to shot. However, they also measure other phenomena that are irrelevant to the far field. For example, waves that go up and down the wires and chains that connect the airguns and the NFH to floatation devices. To separate signal from noise in NFH data it is useful to be able to distinguish an airgun bubble signature from additive noise such as waves in the chains and wires. With an ability to reproduce airgun signatures from a small number of key parameters, such as pressure, depth, exact timing, water temperature and salinity, and air temperature we can separate signal and noise in NFH data. To estimate these key parameters, shot by shot, we can use the NFH data. Instead of a linear inversion with thousands of unknowns, we would rather solve a nonlinear inversion with just a few unknowns. While this methodology is our ultimate goal, we have not yet applied the airgun modeling method that we are developing to NFH data. In this progress report, we try to reproduce the library signature in Figure 4. In this report, our goal is to achieve an accurate model of the bubble convolved with the source force in such a manner that requires few modeling parameters.

MIE SCATTERING

Airgun bubbles are thermodynamic oscillators that radiate acoustic waves. Other oscillators radiate electromagnetic waves. Mie scattering (Mie, 1908) theory predicts scattering of electromagnetic (EM) waves such as radar from metalic objects such as airplanes.

Airgun bubbles and Mie scatterers are both low-cut filters. At low frequencies, there is neither radiation of acoustic waves from an airgun nor scattering of EM waves from small objects. At high frequencies, the airguns fully convert the force of compressed air to acoustic waves and large objects reflect all the EM waves with much smaller wavelength.

The amplitude of the generic Mie scattering plotted as a function of frequency is shown in Figure 5(b). When compared to the spectrum of the library airgun signature in Figure 5(a), it is apparent that while the data spectrum exhibits the shape of a bandpass filter and the modeled spectrum from Mie theory exhibits the shape of low cut filter, the spectra between the low and high frequencies (5-100 Hz) are quite similar in shape. In Figure 6 we observe that Mie scattering spectra is positive real. Positive real wavelets are also minimum phase (Claerbout, 1976). We expect the coupling of source force to acoustic waves to be minimum phase because we expect it to be causal both ways (Kjartansson, 1979). We are not sure about the significance of positive-realness besides insuring minimum-phase. Possibly, positive realness may tell us about the entropy; predict that the (causal) inverse of a (causal) physical process is possible when energy is considered but not possible when entropy is considered. In other words, converting an acoustic wave back to force that would compress air back into an airgun would be causal if it happens, but it would never happen.

While we do not fully understand the reason for the spectral similarity (Figure 7), we believe that it results from the underlying fact that both Mie scatterers and airgun bubbles are radiating oscillators. There are two questions that require justification. One is that the physics are completely different; the airgun is thermodynamic-acoustic, while Mie is electromagnetic (EM). How can we use one for the other? The other question is how can we use scattering for sourcing. The second question is easier. Babinet's principle (Born and Wolf, 1999) states that scattering theory is applicable to radiation from a source.

The justification of the first question (different physics) is more difficult. The governing equations are Maxwell equations on one side and thermodynamics, Navier Stokes, and acoustics on the other. In one side the scatterer size is comparable to the wavelength of resonance. On the other side, the bubble size is much smaller than the wavelength of the acoustic waves that has the same period. We are aware of this need for justification. We therefore collaborate with researchers in the department of geophysics at Stanford University who are developing a physics-based forward-model of the airgun-bubble coupled system. The plan is to adjust or replace the Mie spectra that we are now using with spectra of wavelets that come from their physics-based model. For now, we hope that the justification may first be because it works and we

will later explain why it works. However, we admit that we are not sure that Mie scattering is a workable analogy.

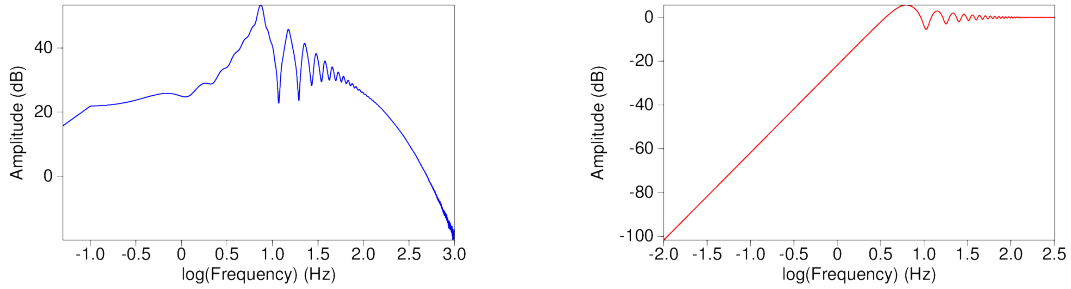

(a) (b)

Figure 5: The library airgun signature spectrum (a) and the amplitude spectrum modeled via Mie scattering theory (b). Note that the signature of the library airgun is a bandpass filter while that of the Mie modeling is a low-cut filter. It means that in addition to coupling which limits the low frequency content of an airgun there is another factor that limits its high frequency content. [**ER**]

METHOD

Note that from this point, we refer to the spectrum modeled via Mie scattering theory as 'Mie' and the library air gun signature as 'library'.

Our general methodology for debubbling the library spectrum is to first warp the spectrum shown in Figure 5(b) (a generic Mie spectrum) to the air gun library spectrum in Figure 5(a). After we compute an adequately warped amplitude spectrum, we then observe the time domain wavelet of this warped Mie spectrum using Kolmogoroff spectral factorization. The justification is that we know that the air gun library trace is minimum phase as shown in Figure 7. With the spectrum and the time domain wavelet, we attempt to debubble the library air gun signature.

Warping Mie to library signature

As stated above, in order to fit the Mie spectrum to the library spectrum, we decide to use a warping approach. That is, we need to find a mapping from a point in the mie space (x, m) to the library space (f, d). More formally, we need to find mappings between the Mie frequency to the library frequency as expressed in equation 1 and Mie amplitude to library amplitude as expressed in equation 2.

$$x \mapsto f \tag{1}$$

$$m \mapsto d \tag{2}$$

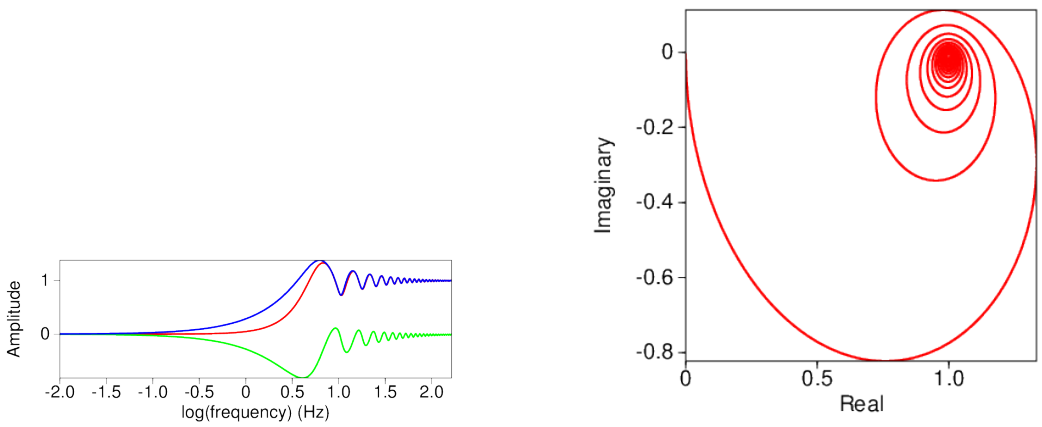

(a) (b)

Figure 6: Analysis of the spectrum modeled with Mie scattering theory. (a) The real part (red), the imaginary part (green) and the amplitude spectrum (blue). (b) The complex hodogram. Note from the hodogram and the real part that the signal is positive real. [**ER**]

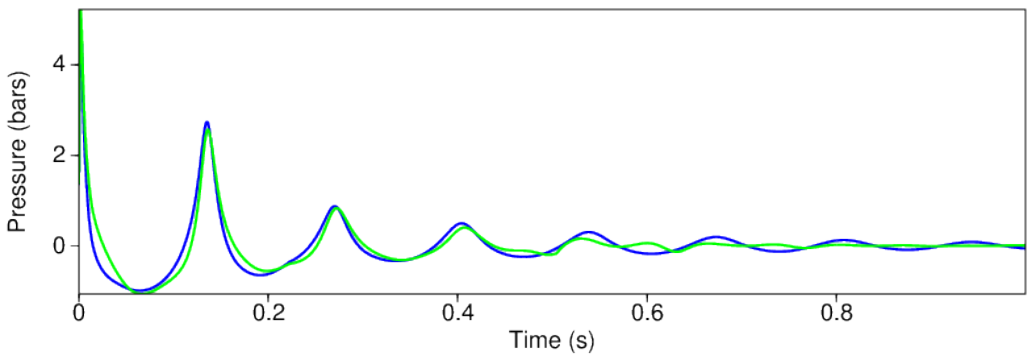

Figure 7: Overlay of the minimum phase equivalent of the library signature (green) and the library signature (blue). The minimum phase equivalent was obtained via Kolmogoroff spectral factorization. The library signature is very close to minimum phase. [**ER**]

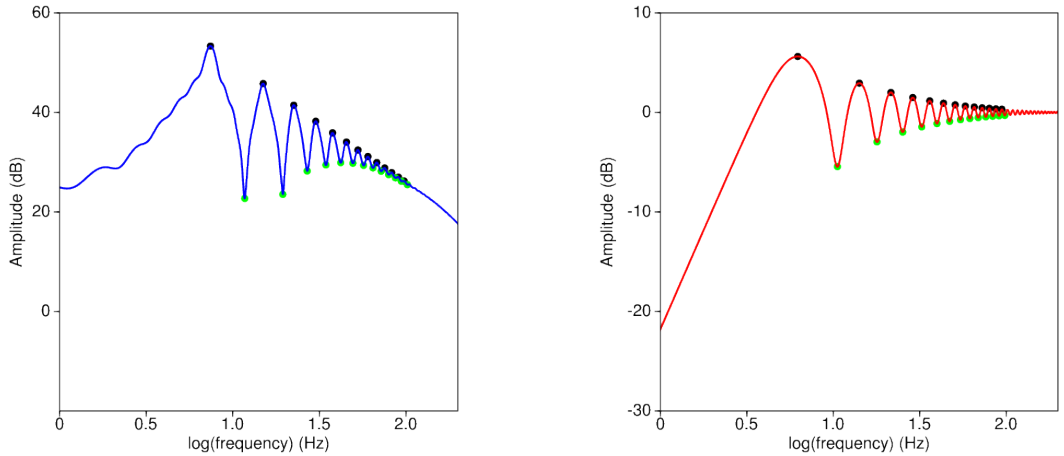

(a) (b)

Figure 8: The control points for the warping of the amplitude spectrum modeled via Mie scattering theory (b) to the library airgun signature spectrum (a). [**ER**]

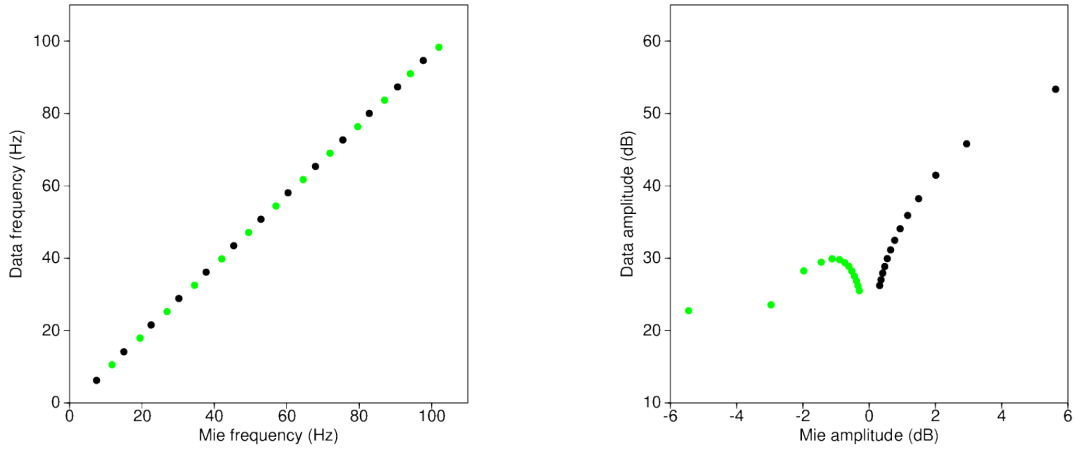

(a) (b)

Figure 9: The cross plots of (a) Mie frequency and the library air gun frequency and (b) Mie amplitude and the library air gun amplitude. Note that as in Figure 8, the black points denote the maxima and the green points denote the minima. (a) shows that we can warp the frequencies but not the amplitudes. This is because the amplitudes are affected by the spectra of a bandlimited source force function and the Mie spectra is for an infinte-band impulse. [**ER**]

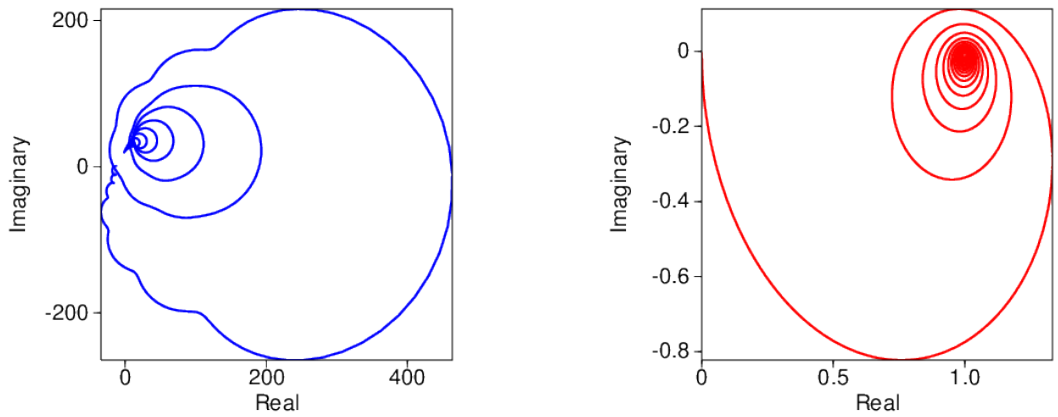

(a) (b)

Figure 10: The library airgun complex hodogram (a) and the complex hodogram of the spectrum modeled by Mie scattering theory (b). Note that the Mie wavelet is positive real and the library wavelet is almost positive real. We suspect that the deviation of the library wavelet from positive-real as well as the wobbliness of the hodogram in low frequencies (where it starts at zero real and zero imaginary) are due to the limitations of estimating airgun signature from experimental data. Mainly, additive low frequency noise in the experimental data and the fairly short recording time of just one second. [**ER**]

While we desire to fit each and every point from the Mie to the library spectrum, we realize that this will only be possible with many fitting terms due to the differences between the two spectra. Therefore, instead of fitting each and every point, we decide to focus on fitting the maxima and minima of the spectra. In other words, we use these points as our "control points". In Figures 8(a) and 8(b) the picked control points are shown where the black points denote the maxima and the green the minima. To get an idea of the mathematics that potentially describe the mappings of the Mie maxima and minima to the library, maxima and minima, we create cross plots of x against f in Figure 9(a) and m against d in Figure 9(b). Once again, in these figures, the green and black points denote the minima and maxima respectively.

Frequency warping

We observe that in Figure 9(a), the mapping is nearly linear and that we we can define the mapping from Mie frequency (x) to the library frequency (f) as:

$$x = bf \tag{3}$$

Using a simple weighted least-squares regression, we can estimate our b parameter. With b, we can then map the Mie frequencies to the data frequencies.

Amplitude warping

Once we have achieved this mapping from Mie frequency (x) to data frequency (f), we can then begin to warp the amplitudes. From Figure 9(b) we observe that the mapping is not linear and therefore may require several parameters. We attribute the complexity of this mapping to the fact that in our Mie modeling we have not taken into account the source force that is present on the library wavelet giving its band pass filter shape. The Mie spectrum, on the other hand, is a low-cut filter and therefore its complex hodogram does not converge to zero as is evident in Figure 10(b). Applying a source force to the Mie spectrum would make this mapping much more linear. The source force function is a convolution operator that multiplies the coupling to generate the library wavelet. Because we warp the amplitudes in the log domain, this multiplication becomes an addition. Therefore, we can describe the mapping between the Mie amplitude and data amplitude as:

$$d(f) \approx m_{warped}(f) = a_m m(x(f)) + s(f) \tag{4}$$

where d is the library airgun signature (data), a_m is a scale factor to be applied to the unwarped Mie spectrum, m is the unwarped Mie spectrum and $s(f)$ is the source force. We parameterize the source force $s(f)$ as

$$s(f) = \sum_{i=-1}^{2} a_i f^i \tag{5}$$

where a_i denotes the coefficients of the $s(f)$ polynomial.

Once again, we can use a linear regression in order to estimate a_m, a_{-1}, a_0, a_1 and a_2 where we define our residual as:

$$r_i = d_i - a_m m(f_i) - \frac{a_{-1}}{f_i} - a_0 - a_1 f_i - a_2 f_i^2 \tag{6}$$

Therefore, our fitting goal is to minimize this residual.

RESULTS

Warping results

After estimating the frequency, amplitude and source force parameters described in the previous section and warping the Mie spectrum to the library spectrum, we obtain the warped Mie spectrum shown in Figure 11. In this figure, it is clear that while we have fit several maxima and minima quite well, we fail to fit the 8Hz low frequency maxima. Furthermore, we can observe that at low frequencies the spectra seem to agree, but then at the higher frequencies they mismatch This is due to a weighting operator that we applied to the residual in estimating our frequency fitting parameter b (3). This is quite evident in Figure 12 where the slope of the red line is the estimated b parameter. The weighting operator was chosen to fit the first four maxima and minima and the remaining elements of the diagonal were left as zeros.

We use Figure 13 as a quality-check for our fit. Instead of showing the relationship between x and f, m and d, these plots show the mapping between the minima and maxima of the warped Mie and the minima and maxima of the library signature. As expected the mapping between x_{warped} and f shown in Figure 13(a) is still linear. In Figure 13(b) we observe that warping the Mie spectrum with the incorporated source force did greatly improve the mapping, but it is not quite linear. This is mostly due to the use of our weighting operator which gives us a better fit of the lower frequencies.

Time domain wavelets

Now that we have warped the Mie spectrum to the data spectrum, we can find the time-domain minimum-phase equivalent wavelet using Kolmogoroff spectral factorization. Performing this computation gives us the time-domain Mie wavelet shown in Figure 14. Comparing this wavelet to the library wavelet also shown in Figure 14, we see that the Mie wavelet in general resembles that of an airgun signature. Clearly, it shows bubble oscillations and has a peak to bubble ratio comparable to that of the library wavelet. Unfortunately, the deep second bubble oscillation tells us that this result is non-physical as the energy of the bubble should be decreasing as time

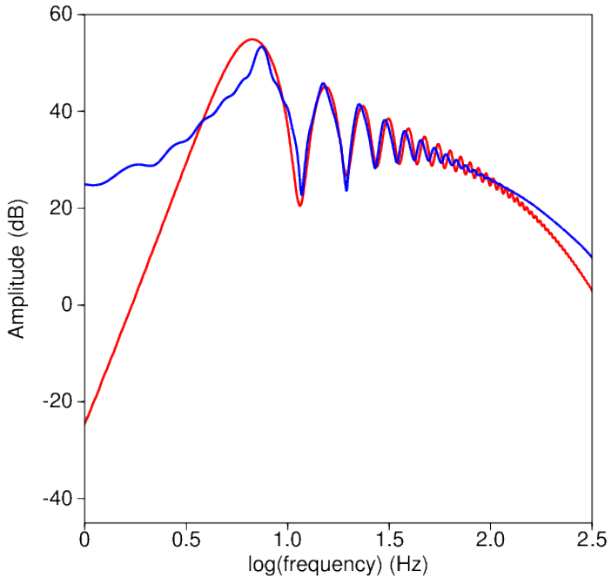

Figure 11: Warping result. [**ER**]

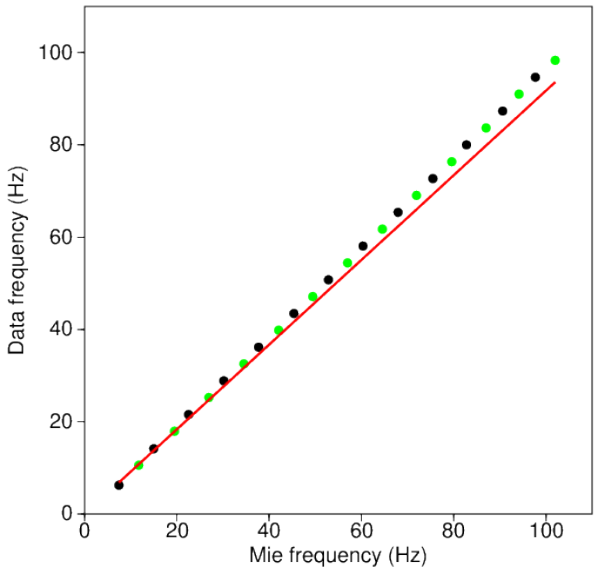

Figure 12: The fitted cross plots of Mie frequency and the library air gun frequency. Note that as in Figure 8, the black points denote the maxima and the green points denote the minima. [**ER**]

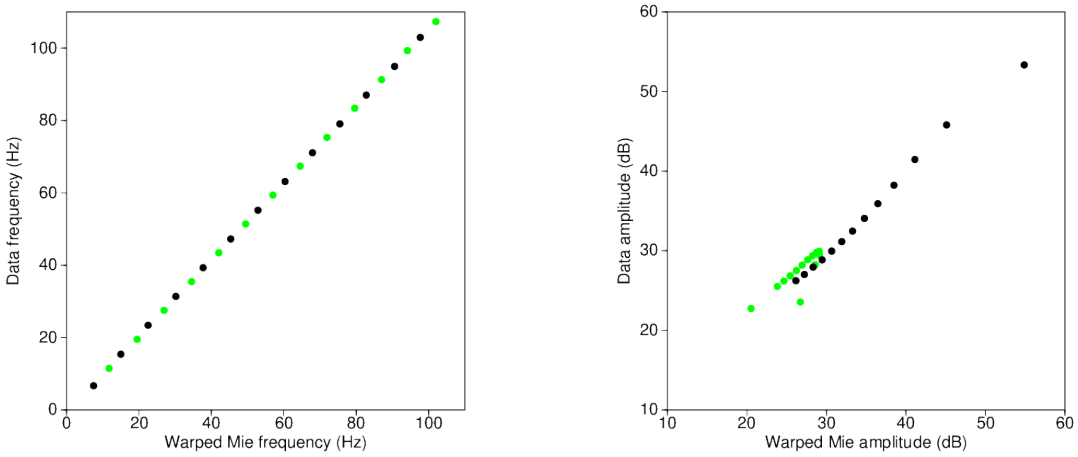

(a) (b)

Figure 13: The cross plots of (a) warped Mie frequency and the library air gun frequency and (b) warped Mie amplitude and the library air gun amplitude. Comparing (b) with Figure 9(b), we observe that the mapping is now nearly linear between the amplitudes. [**ER**]

increases. We consider this result as a preliminary finding on our path to finding a better wavelet.

Designature

With the warped Mie spectrum, we can now deconvolve the bubble from the library airgun signature. We perform this deconvolution on the amplitude spectrum in the dB domain. The designatured amplitude spectrum can be seen in Figure 15(a). In performing the deconvolution, a pre-whitening factor of 0.1 was used. From this figure, we observe the remaining bubble spectrum from approximately 8-100 Hz.

Once again, to find the minimum-phase time-domain equivalent wavelet we use Kolmogoroff spectral factorization. The resulting designatured time-domain wavelet is shown Figure 15(b). While it appears that some of the bubble signature was removed as a result of the deconvolution, most of it remains due to the misfit between the Mie and library wavelets.

DISCUSSION AND CONCLUSION

In this progress report, we have shown that by warping the spectrum computed by Mie scattering theory and then finding its minimum phase equivalent time-domain

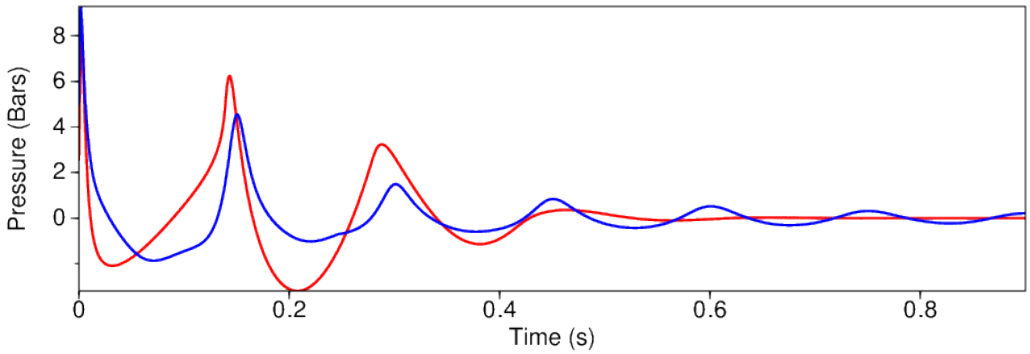

Figure 14: The comparison of the time-domain warped Mie wavelet (red) and the original library wavelet (blue). We are not satisfied with this result; the bubble shape and period fits are not perfect and make the result unsatisfactory. The peak to bubble ratio is under estimated, and the second trough is deeper than the first trough, which is non-physical. Nevertheless, we show this result in this progress report. [**ER**]

wavelet by Kolmogoroff spectral factorization we can obtain a time-domain wavelet that resembles an air gun signature. With this wavelet, we have attempted to designature a library airgun signature. The results are encouraging. However, as stated previously, we are not satisfied with the wavelets shown in Figures 14-15(b) as they are non-physical. We believe that the results we have obtained are non-physical due to the fundamental differences between the Mie spectrum and the library spectrum and therefore. These differences force us to rely heavily on warping to get a signature that resembles one of an airgun. To overcome this, in the future we will look into alternative Mie formulations and attempt to warp the spectrum in the complex hodogram domain. This will ensure that the Mie spectrum is positive real and also will have the same amplitude and phase spectrum as the library airgun spectrum. We believe that this will resolve the matches in the bubble period.

ACKNOWLEDGEMENTS

The authors would like to thank Dolphin Geophysical and Chelminski associates for the permission to show the lake data. They would also like to thank Avishai Ben David for observing that the airgun source spectra resemble Mie scattering spectra and Ettore Biondi for thoughtful discussions

REFERENCES

Born, M. and E. Wolf, 1999, Principles of optics: Cambridge University Press.

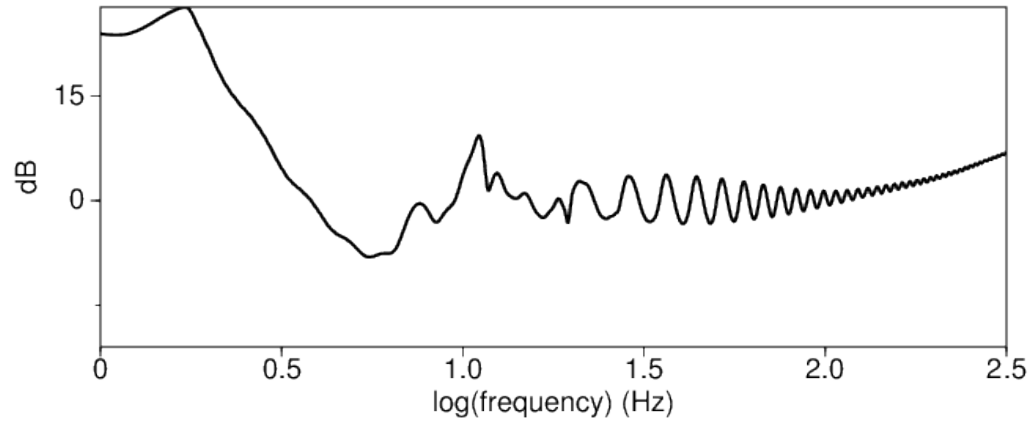

(a)

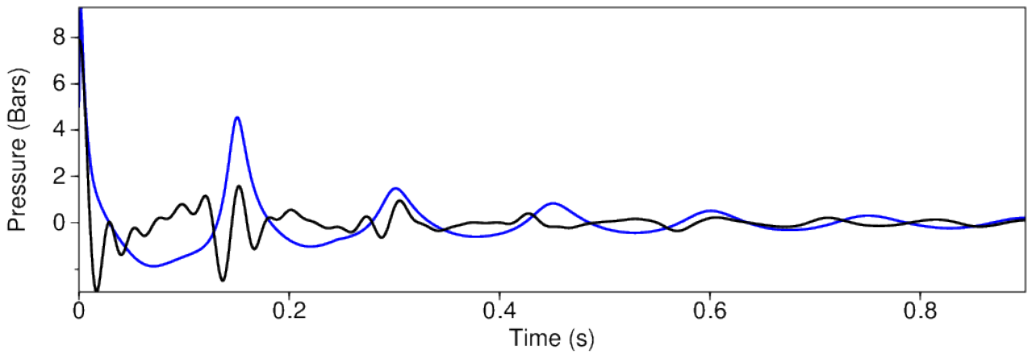

(b)

Figure 15: (a) The designatured amplitude spectrum and (b) the minimum-phase equivalent of the designtured amplitude spectrum computed via Kolmogoroff spectral factorization. In computing the designature, a pre-whitening factor of 0.1 was used. [**ER**]

Claerbout, J., 1976, Fundamentals of geophysical data processing with applications to petroleum prospecting: Blackwell Scientific Publications.

Kjartansson, E., 1979, Attenuation of seismic waves in rocks and applications in energy exploration: PhD thesis, Stanford University.

Mie, G., 1908, Beitrge zur optik trber medien, speziell kolloidaler metallsungen: Annalen der Physik, **330**, 337–445.

Ziolkowski, A., G. Parkes, L. Hatton, and T. Haugland, 1982, The signature of an air gun array: Computation from near-field measurements including interactions: Geophysics, **47**, 1413–1421.